Appl Biochem Biotechnol
DOI 10.1007/s12010-017-2404-9

Metal-Chelate Immobilization of Lipase onto Polyethylenimine Coated MCM-41 for Apple Flavor Synthesis

Armin Sadighi[1] · Seyed Farshad Motevalizadeh[2] · Morteza Hosseini[3] · Ali Ramazani[4] · Lena Gorgannezhad[5] · Hamid Nadri[6] · Behnaz Deiham[7] · Mohammad Reza Ganjali[8] · Abbas Shafiee[9] · Mohammad Ali Faramarzi[10] · Mehdi Khoobi[9,11]

Received: 16 July 2016 / Accepted: 11 January 2017

Abstract An enzyme immobilized on a mesoporous silica nanoparticle can serve as a multiple catalyst for the synthesis of industrially useful chemicals. In this work, MCM-41 nanoparticles were coated with polyethylenimine (MCM-41@PEI) and further modified by chelation of divalent metal ions (M = Co^{2+}, Cu^{2+}, or Pd^{2+}) to produce metal-chelated silica nanoparticles

This paper is dedicated to the memory of Professor Abbas Shafiee.

Electronic supplementary material The online version of this article (doi:10.1007/s12010-017-2404-9) contains supplementary material, which is available to authorized users.

✉ Mohammad Ali Faramarzi
faramarz@tums.ac.ir

✉ Mehdi Khoobi
m-khoobi@tums.ac.ir; Mehdi.khoobi@gamil.com

[1] Department of Biomedical and Pharmaceutical Sciences, College of Pharmacy, University of Rhode Island, Kingston, RI 02881, USA

[2] Particulate Fluids Processing Centre, School of Chemistry, The University of Melbourne, Melbourne, VIC 3010, Australia

[3] Department of Life Science Engineering, Faculty of New Sciences and Technologies, University of Tehran, Tehran, Iran

[4] Department of Chemistry, University of Zanjan, P.O. Box 45195-313, Zanjan, Iran

[5] School of Natural Sciences, Griffith University, Nathan Campus, QLD 4111, Australia

[6] Faculty of Pharmacy, Shahid Sadoughi University of Medical Sciences, Yazd, Iran

[7] Division of Microbiology, Department of Pathobiology, School of Public Health, Tehran University of Medical Sciences sTUMS, Tehran, Iran

Published online: 13 February 2017

(MCM-41@PEI-M). *Thermomyces lanuginosa* lipase (TLL) was immobilized onto MCM-41, MCM-41@PEI, and MCM-41@PEI-M by physical adsorption. Maximum immobilization yield and efficiency of 75 ± 3.5 and 65 ± 2.7% were obtained for MCM@PEI-Co, respectively. The highest biocatalytic activity at extremely acidic and basic pH (pH = 3 and 10) values were achieved for MCM-PEI-Co and MCM-PEI-Cu, respectively. Optimum enzymatic activity was observed for MCM-41@PEI-Co at 75 °C, while immobilized lipase on the Co-chelated support retained 70% of its initial activity after 14 days of storage at room temperature. Due to its efficient catalytic performance, MCM-41@PEI-Co was selected for the synthesis of ethyl valerate in the presence of valeric acid and ethanol. The enzymatic esterification yield for immobilized lipase onto MCM-41@PEI-Co was 60 and 53%, respectively, after 24 h of incubation in *n*-hexane and dimethyl sulfoxide media.

Keywords Lipase immobilization · Mesoporous silica nanoparticles · Polyethylenimine · Metal chelation · Esterification

Introduction

The biocatalytic functions of enzymes through regioselective, enantioselective, and stereoselective conversion of chemicals into valuable products, as well as their specificity and activity under mild physical conditions (e.g., moderate pH and temperature), make enzymes remarkable catalytic candidates in the food, chemical, pharmaceutical, cosmetics, perfumery, and tannery industries [1–5]. One of the main concerns in large-scale catalytic processes is finding a way to decrease the unit cost of each enzymatic step [6–8]. The immobilization of a catalyst on the surface of an inert support, especially one that exhibits high physical and chemical stability under diverse reaction conditions, can decrease the economic investment due to the potential for running the catalytic reaction in multiple rounds while simultaneously harnessing the beneficial biocatalytic properties of enzymes [9, 10]. Furthermore, immobilized enzymes show higher mechanical and physical stability than do free enzymes in the presence of harsh chemical and microbial substances, along with resistance to extremes of pH and temperature. Several enzyme immobilization strategies have been developed, including physical entrapment and/or adsorption [11], covalent binding, cross-linking [12], reversed micelle, hydrophobic ion pair [13], and bio-affinity ligation [14]. Combinations of immobilization methods have been developed, which avoid the drawbacks of using just a single approach. Decreasing the risk of enzyme leakage by cross-linking of a physically adsorbed enzyme [13] and increasing the immobilization capacity using covalent bonding that is enhanced by further adsorption to metal chelated ions [5] are examples of combinative

[8] Biosensor Research Center, Endocrinology and Metabolism Molecular-Cellular Sciences Institute, Tehran University of Medical Sciences, Tehran, Iran

[9] Nanobiomaterials Group, Pharmaceutical Sciences Research Center, Tehran University of Medical Sciences, Tehran 1417614411, Iran

[10] Department of Pharmaceutical Biotechnology, Faculty of Pharmacy and Biotechnology Research Center, Tehran University of Medical Sciences, P.O. Box 14155-6451, Tehran 14176, Iran

[11] Department of Pharmaceutical Biomaterials and Medical Biomaterials Research Center, Faculty of Pharmacy, Tehran University of Medical Sciences, Tehran, Iran

immobilization methods. Enzyme purification and immobilization mediated by chelated transition metals were introduced by Porath and co-workers [15, 16]. Subsequent research has confirmed the potential of coordination chemistry in enzyme immobilization [17–21] (Table S1).

Lipases (triacylglycerol ester hydrolases, EC 3.1.1.3), which are responsible for hydrolyzing triacylglycerol into glycerol and free fatty acids, are extensively used in the food and pharmaceutical industries. In addition, lipases are widely applied in fields utilizing enzymatic processes due to their broad range of catalytic activities, such as regioselective acetylation, acidolysis, aminolysis, alcoholysis, and one-step interesterification [22, 23]. Lipases generally adopt a common α/β hydrolase fold composed of a catalytic domain and a cap or lid domain. The catalytic triad (Ser-His-Asp or Ser-His-Glu) is structurally conserved among all kinds of lipases and covered by an α-helix lid. This subdomain is responsible for the transition of lipase from the closed form (i.e., with an inaccessible active site) to the open form, which facilitates binding of the substrate to the active site [24–28].

Lipases have shown promising capability in a wide variety of chemo-enzymatic processes, including epoxidation of fatty acids and phenolic compounds [29], oxidation and epoxidation of alkenes, Baeyer–Villiger oxidation of cyclic ketones to lactones [30], and green synthesis of optically pure pharmaceuticals from a racemic mixture of compounds in nonaqueous continuous reactions [31].

Up to now, different supports and immobilization techniques were exploited for lipase confinement [32]. Among them, inorganic supports have emerged as promising candidates due to their mechanical and chemical stability against the influence of organic solvents and microbial agents [2]. Over the last two decades, a range of inorganic supports has been employed for lipase immobilization [33–37]. Among them, MCM-41 is one of the most popular scaffolds applied to enzyme immobilization, especially by physical adsorption [38]. Reasons for the popularity of MCM-41 include (i) large pore size, which allows loading of bulky enzymes into the pore, thus protecting the protein from denaturation; (ii) the presence of silanol groups on the surface of MCM-41 facilitating the immobilization of enzymes via hydrogen bonding [39, 40]; and (iii) mechanical stability, which protects immobilized biocatalyst against abrasion and breaking [41–44]. Moreover, introducing suitable polymers on the surface of ordered MSNPs and chemically modifying the scaffold can provide a more appropriate environment for enzyme immobilization [4]. These outstanding features make MCM-41 as an omnipresence material with a wide range of application in different field of sciences [45–47].

In this study, physical adsorption of lipase through chelated divalent metal ions on the surface of PEI-coated MCM-41 (MCM-41@PEI) was successfully accomplished. Multiple available amine branches of PEI on the surface of MCM-41 were exploited as metal ion chelators. Three different metal ions (Co^{2+}, Cu^{2+}, and Pd^{2+}) were loaded on the supports to obtain a suitable adsorption capacity. These metal ions facilitate multipoint enzyme adsorption through thiol group of cysteine (Cys), indole group of tryptophan (Trp), and imidazole ring of histidine (His) present on lipase surface. Optimum pH and temperature, storage stability, and reusability of the immobilized lipase were compared with the free enzyme. Moreover, esterification reaction of ethanol and valeric acid catalyzed by the best lipase immobilized system was investigated for the synthesis of ethyl valerate (green apple flavor) in various organic solvents.

Materials and Methods

Chemicals

Hyperbranched polyethyleneimine (PEI, MW = 60,000), [3-(2,3-epoxypropoxy)propyl] trimethoxysilane (EPO, 98% purity) and *p*-nitrophenyl butyrate (*p*-NPB) were purchased from Sigma-Aldrich (St. Louis, MO, USA). Cetyltrimethylammonium bromide (CTAB), tetraethyl orthosilicate (TEOS), aqueous ammonia solution (28 wt%), valeric acid, dimethyl sulfoxide (DMS), *n*-hexane, and all other solvents were obtained from Merck (Darmstadt, Germany). Palladium chloride ($PdCl_2$), copper (II) chloride ($CuCl_2$, 99% purity), and cobalt (II) chloride ($CoCl_2$, 97% purity) were purchased from Merck AG. *Thermomyces lanuginos*a lipase (TLL) was kindly donated by Novozymes (Bagsvard, Denmark).

Preparation of PEI Grafted MCM-41 and Metal Loading

MCM-41@PEI was prepared according to a procedure described previously [2]. Briefly, a solution of CTAB (13 g) in deionized water (167 mL), aqueous ammonia (163.7 mL), and absolute ethanol (131.5 mL) was stirred at room temperature for 1 h. Next, TEOS (49.6 g) was added dropwise to the mixture and stirred vigorously for 2 h. Then, the white precipitate was filtered, washed with deionized water, and dried at 60 °C for 24 h. The organic template was removed via calcination of as-prepared MCM-41 under an oxygen atmosphere by heat treatment at a rate of 1 °C min^{-1} up to 600 °C using high-temperature oven (LHT 6/60, Carbolite, UK). This temperature was maintained for 6 h.

For covalent grafting of PEI on the surface of MCM-41, PEI (3.7 g) was added to 150 mL dry toluene. Then, EPO (1.1 mL) was added and allowed to react at 80 °C for 24 h. Next, a mixture of MCM-41 (5 g) and ethanol (25 mL) was added and stirred at 80 °C for a further 24 h. The final product, MCM-41@PEI, was then filtered and washed several times by deionized water and ethanol. The obtained product was soxhleted with ethanol for 24 h to remove physically bonded compounds, filtered, and dried at 50 °C for several days. Different metal ions were then chelated on the surface of MCM-41@PEI by the aid of high amount of amine groups. Briefly, a solution containing 0.6 mmol of metal ion ($PdCl_2$, $CuCl_2$, and $CoCl_2$,) in acetonitrile (25 mL) was prepared. MCM-41@PEI (300 mg) was added to the solution and stirred under nitrogen atmosphere for 48 h. The final products, denoted MCM-41@PEI-M, were filtered and washed with acetonitrile and acetone separately and air-dried for 24 h.

Characterization

Thermogravimetric analysis (TGA) of the prepared supports was carried out using a TGAQ50, TA Instruments. A heating rate of 10 °C min^{-1} was used from room temperature to 800 °C under an argon flow. The X-ray diffraction (XRD) pattern was executed using XPert MPD advanced diffractometer employing Cu Kα (λ = 1.54 Å) radiation at room temperature in the 2θ range from 4° to 120°. Fourier transform infrared (FT-IR) analysis was recorded on Nicolet FT-IR Magna 550 spectrographs (KBr disks). The surface morphology of the samples was investigated by scanning electron microscopy (SEM) using a VEGAII TESCAN with an

acceleration voltage of 15 kV. Sample preparation for transmission electron microscopy (TEM, CM30 Philips) was done by placing a droplet (1 μL) of sample dispersion latex along with a droplet of water on a copper grid covered by Formvar foil (200 mesh) and analyzed after drying. Energy-dispersive X-ray spectroscopy (EDX) was performed with a Philips XL 30 X-Ray spectrometer. Dynamic light scattering (DLS) was applied to determine the particles size (DTS Ver. 4.20). Pore size and surface area were measured by nitrogen sorption (BELSORP Mini, BELJapan Inc.) at 77 K. Prior to experiment, all samples were degassed to 0.1 Pa with MCM-41 and MCM-41@PEI kept at 300 °C and 100 °C for 2 h, respectively. The surface area was calculated according to the Brunauer–Emmett–Teller (BET) method, while pore size distribution and pore volume were estimated using the BJH model and adsorption curve, respectively [2].

Lipase Immobilization and Enzyme Assay

Prior to enzyme immobilization on supports, TLL was refined from octyl-sepharose beads by stirring in sodium phosphate buffer (25 mM, pH 7.4) containing CTAB (0.6% *v*/*v*) for 1 h at room temperature. The enzyme solution was then filtered and rinsed three times with the same buffer. The essential time for maximum immobilization efficiency was determined by immersing MCM-41@PEI-M (10 mg) containing lipase (1 mL, equal to 5 U) in phosphate buffer (0.1 M, pH 7.0) followed by incubating at 25 °C for 15–90 min.

Lipase immobilization was examined according to physical adsorption of enzyme onto MCM-41@PEI-M. The immobilization yield (IY) and immobilization efficiency (IE) were calculated as IY (%) = $[(Y_0–Y_1) / Y_0] \times 100$ and IE (%) = $[E_1 / E_0] \times 100$, where Y_0 and Y_1 indicate the amounts of total and unbound enzyme on the supports, respectively, whereas E_0 and E_1 represent the total and immobilized enzyme activity, respectively.

p-NPB was used as substrate to measure the catalytic activity of free and immobilized TLL as described previously [2, 5]. Briefly, 0.1 mL of free and 10 mg of immobilized lipase (equal to 5 U) were added to 0.9 mL *p*-NPB solution [0.4 mM in sodium phosphate buffer (100 mM, pH 7.4)]. This mixture was incubated at 37 °C for 10 min, and the absorbance was measured at 410 nm using a UV-visible spectrophotometer (UVD 2950, Labomed Inc., Culver City, CA, USA). The amount of enzyme releasing 1 μmol *p*-NPB min^{-1} was defined as one unit (U) of enzyme activity. The total amount of free and immobilized protein were measured by the Bradford assay at 595 nm based on the bovine serum albumin standard line (12.5–400 μg/mL) [48].

Optimum pH and Temperature for Immobilized Lipase Activity

Free and immobilized lipase were incubated in 100 mM citrate-phosphate (pH 3–7), Tris-HCl (pH 8), and glycine-NaOH buffers (pH 9–10) at 37 °C for 1 h to investigate the effect of pH on enzyme consistency. The relative enzyme activity at different pH values were estimated by determining the residual enzyme activity compared to the initial amount. To study the thermal stability of the free and immobilized lipase, the enzyme was placed in a water bath at temperatures ranging from 15 to 75 °C for 1 h. The residual lipase activity was then measured to clarify the optimum activity for free and immobilized lipase.

Storage Stability and Reusability of Immobilized Lipases

The free and immobilized lipases were kept at 37 °C for 14 days to analyze the long-term storage stability. After each day, the remaining activity was measured and compared to the initial activity at the beginning of the experiment. To investigate the reusability potential of the immobilized lipase, a substrate solution was added to the immobilized enzyme and the activity measured after 10 min. At the end of each run, the reaction mixture was separated from the support and the support washed three times with phosphate buffer (100 mM, pH 7.4). To continue the catalytic process, the immobilized enzyme was reincubated with the substrate for subsequent catalytic runs. In this method, the lipase activity was determined as 100% at the first run and as relative activity during succeeding runs.

Enzymatic Synthesis of Ethyl Valerate by Free and Immobilized Lipase

Lipase immobilized on MCM-41@PEI-Co as the best biocatalyst was evaluated in esterification of ethyl alcohol and valeric acid in organic solvents or free solvent condition. The reaction was initially carried out at different temperatures of 30, 45, and 60 °C for 1, 2, 4, 6, 12, and 24 h with 2:1 M ratio of ethyl alcohol to valeric acid under solvent-free condition and in the presence of the immobilized lipase (5 mg) or free lipase (0.5 mL). The influence of alcohol to acid molar ratio (i.e., 2:1, 1:1, 1:2, 1:3, 1:4, and 1:5) was then studied under the optimal temperature (40 °C). Ratio (4:1 M) of ethyl alcohol to valeric acid was obtained as best ratio under solvent-free condition. In the case of organic solvent, ethanol (4 mmol) and valeric acid (1 mmol) were dissolved in anhydrous DMSO or *n*-hexane (10 mL) in the presence of immobilized lipase (5 mg) or free lipase (0.5 mL). No significant esterification yield was achieved in the absence of enzyme (less than 2%). Finally, the impact of different solvent was assessed under the optimized condition. A mixture of valeric acid and ethyl alcohols in appropriate solvent (15 mL) was shacked at 100 rpm and 40 °C, and heat-inactivated free lipase was used as control (all experiments were performed in triplicate). A simple alkalimetric method was applied to determine the yield of esterification (titration was performed using 0.1 N NaOH, and phenolphthalein was used as an indicator). Valeric acid consumption after a certain time was used to measure the quantity of the synthesized ester.

Results and Discussion

Preparation of MCM-41@PEI-M and Lipase Immobilization

Figure 1a shows the sequential steps required for the preparation of MCM-41, MCM-41@PEI, and MCM-41@PEI-M followed by lipase immobilization onto the porous supports. In this study, MCM-41 was prepared based on hydrothermal method and then calcined to remove any surfactant remaining. The epoxy group of EPO reacted with the amine groups of PEI before being grafted onto MCM-41 through the silanol groups of EPO and hydroxyl groups of MCM-41, thus forming MCM-41@PEI. These amino groups were finally coordinated with different metal ions to enhance the capability of the support for enzyme immobilization. On the one hand, the presence of myriad branches of amine groups on the surface of the support provides

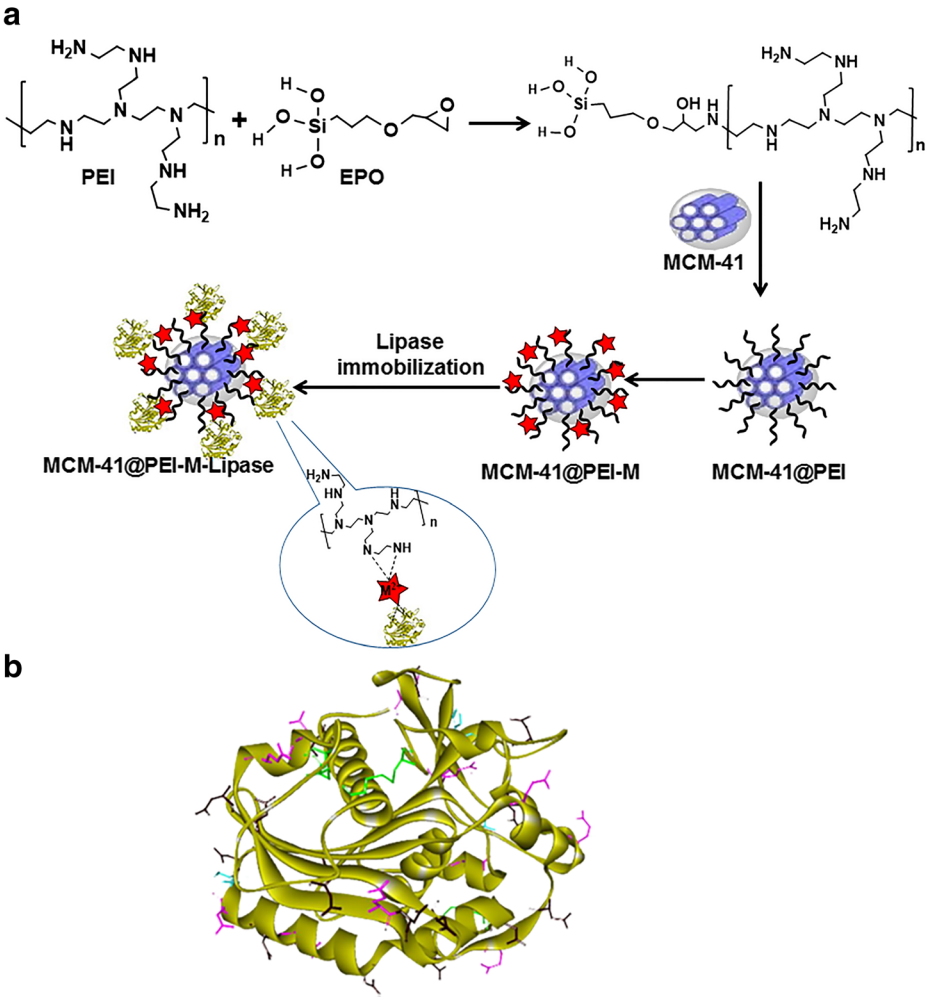

Fig. 1 **a** A schematic illustration for the preparation of MCM-41@PEI-M and lipase immobilization via adsorption. **b** The crystal structure of *Thermomyces lanuginosa* lipase (PDB ID: 1DT3, resolution 2.6 Å). Peripheral amino acids with polar side chains, which are probably involved in enzyme immobilization on the prepared supports, are shown in atomic display style with different colors: histidine (*blue*), cysteine (*green*), glutamic acid (*pink*), and aspartic acid (*brown*). The Accelrys Discovery Studio 4.1 Visualizer was applied to visualize the structure of the TLL model

a perfect condition for enzyme immobilization via electrostatic and dipole-dipole interaction as well as hydrogen bonding. On the other hand, all amino acids on the surface of enzyme with polar side chains, including Cys, Asp, Glu, and His can be coordinated with divalent metal ions. Figure 1b shows the crystallographic structure of TLL (PDB ID: 1DT3, resolution 2.6 Å) and the responsible peripheral amino acids, which are coordinated with metal ions [49].

Characterization of MCM-41, MCM-41@PEI, and MCM-41@PEI-M

The FT-IR spectra of the prepared MCM-41, MCM-41@PEI, and MCM-41@PEI-M are shown in Fig. 2. The absorption band at 467 cm^{-1} is attributed to the bending vibration, while

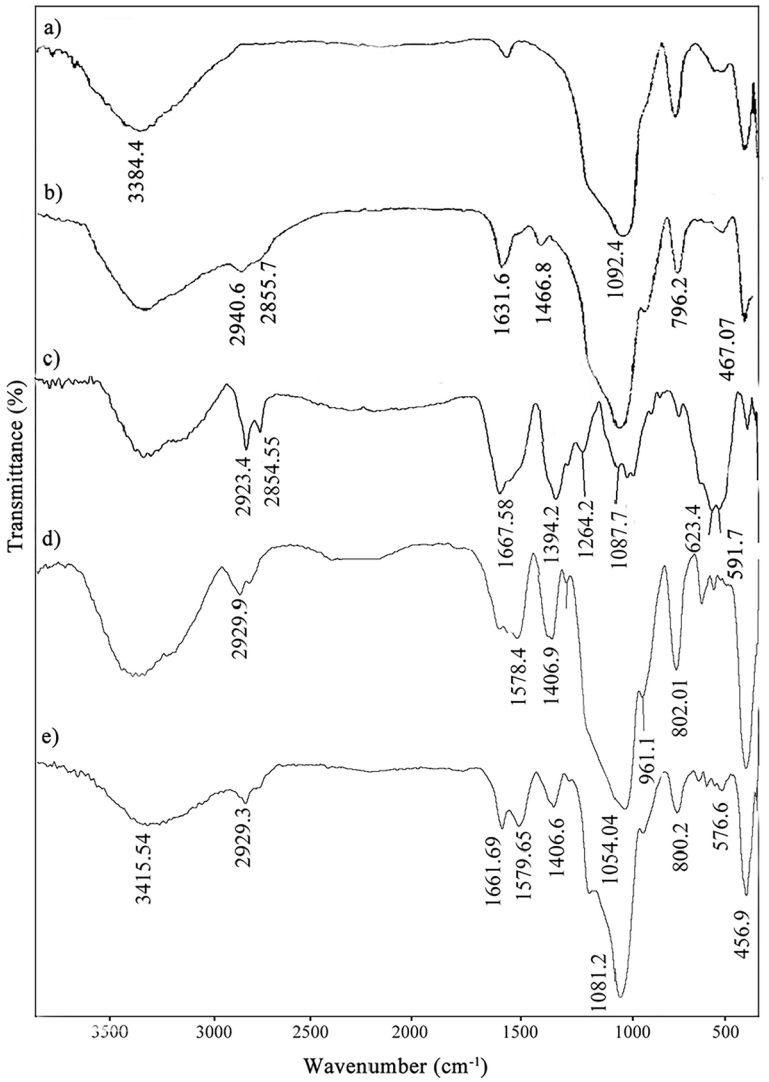

Fig. 2 FT-IR spectra of **a** MCM-41, **b** MCM-41@PEI, **c** MCM-41@PEI-Co, **d** MCM-41@PEI-Cu, and **e** MCM-41@PEI-Pd

those at 796.2 and 1092.4 cm^{-1} are indicative for symmetric and asymmetric stretching vibrations of the Si–O–Si group, respectively [50]. The strong peaks at around 3400 cm^{-1} result from the stretching vibration of OH, which confirms the presence of large numbers of hydroxyl or amine groups on the surface of the prepared supports (Fig. 2a–e). Additionally, the FT-IR spectrum for MCM-41@PEI (Fig. 2b) showed more peaks compared to the bare MCM-41 at 2855 and 1466 cm^{-1} (Fig. 2a). These bands may have arisen from the stretching vibrations for C–H and C–N bonds, respectively. The presence of the C–N bond indicates the successful formation of MCM-41@PEI. The band around 970 cm^{-1} could be attributed to the C-N bending vibration as well. The band around 1570 cm^{-1} could be appeared due to the

symmetric bending vibration of $–NH_2$, and another one at 1630–1670 cm^{-1} (Fig. 2c–e) could be ascribed to the bending vibration of –N(R)H in PEI [51, 52]. The metal complexation could be confirmed by FTIR analyses (Fig. 2c–e). M–N stretching vibrations could be appeared at about 590 (Pd-N) and 450 cm^{-1} (Co-N and Cu-N) [53–55].

Thermogram analysis (TGA) of MCM-41@PEI showed four steps of weight loss (Fig. S1a). At first, 2% of initial weight decreased due to water vaporization at temperatures in the range of 50–105 °C. In the next step, 2.7% weight loss appeared in the range of 105–270 °C because of desorption of physisorbed water that constrained in the hexagonal channels. In the third step, nearly 15% of weight loss happened in the range of 270–400 °C as a result of oxidative decomposition of organic moiety. Finally, 3% of weight loss occurred in the range of 400–800 °C that ascribed from dehydroxylation of the silicate networks [2].

X-ray diffraction analysis (XRD) of MCM-41 showed strong peak at $2\theta = 2.1°$ due to (100) reflection and three weak peaks at $2\theta = 3–6°$, which attributed to (110), (200), and (210) reflections [43]. The observed peaks indicated the formation of highly ordered hexagonally shaped pores in MSNPs. The same peaks with lower intensity were observed for MCM-41@PEI, which confirms the preservation of crystallographic lattice after PEI grafting **(**Fig. S1b**)** [2].

The nitrogen adsorption-desorption profiles of MCM-41 and MCM-41@PEI are presented in Fig. S1c, d, respectively. Specific surface area (BET), pore volume (V_p), and diameter (D_p) were measures, and a summary of results are mentioned in Table S1. The N_2 adsorption-desorption profile of MCM-41 shows IUPAC Type IV isotherm with a step-up in a narrow range of relative pressure (P/Po = 0.2–0.3) corresponding to the capillary condensation of N_2 in uniform hexagonal pores. The same isotherm observed for MCM-41@PEI, which means that PEI uniformly covered MCM-41 pores.

SEM and TEM analyses were applied to study the size and morphology of the MSNPs. SEM results showed that all MSNPs have spherical to near spherical shape and smooth surface in the size range of 200–400 nm (Fig. 3a, c, e**)**. Due to the thin thickness of PEI shell structure around MCM-41, no significant difference was observed in surface geometry of the functionalized MCM-41 as compared to the bare MCM-41 based on SEM images. These images also showed agglomeration arising from the high surface-to-volume ratio for the particles. For further investigation, TEM was carried out to confirm the formation of MSNPs and core–shell structure of MCM-41@PEI. TEM image showed the formation of the regular

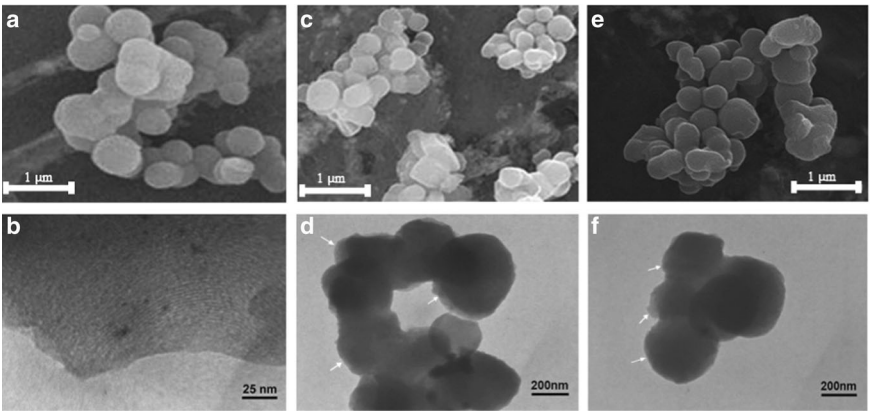

Fig. 3 **a** SEM and **b** TEM images of MCM-41, **c** SEM and **d** TEM images of MCM-41@PEI, **e** SEM and **f** TEM images of MCM-41@PEI-Co

hexagonal array of uniform channels for MCM-41 (Fig. 3b**)** with pore size about 3 nm, which agreed with nitrogen adsorption results [2]. In addition, TEM of MCM-41@PEI and MCM-41@PEI-Co confirmed the formation of a core–shell structure, as shown in Fig. 3d, f. These images also showed agglomeration arising from the high surface-to-volume ratio for the particles. Dynamic light scattering results also revealed that MSNPs size are about 400 nm, which were in good agreement with the results of TEM images (Fig. S2).

The EDX spectra of the three MCM-41@PEI-M supports are shown in Fig. 4**.** The atomic weight ratio of C/N/Si/M were calculated as 22.2:9.7:11.4:9.4, 10.1:8.9:22.8:6.4, and

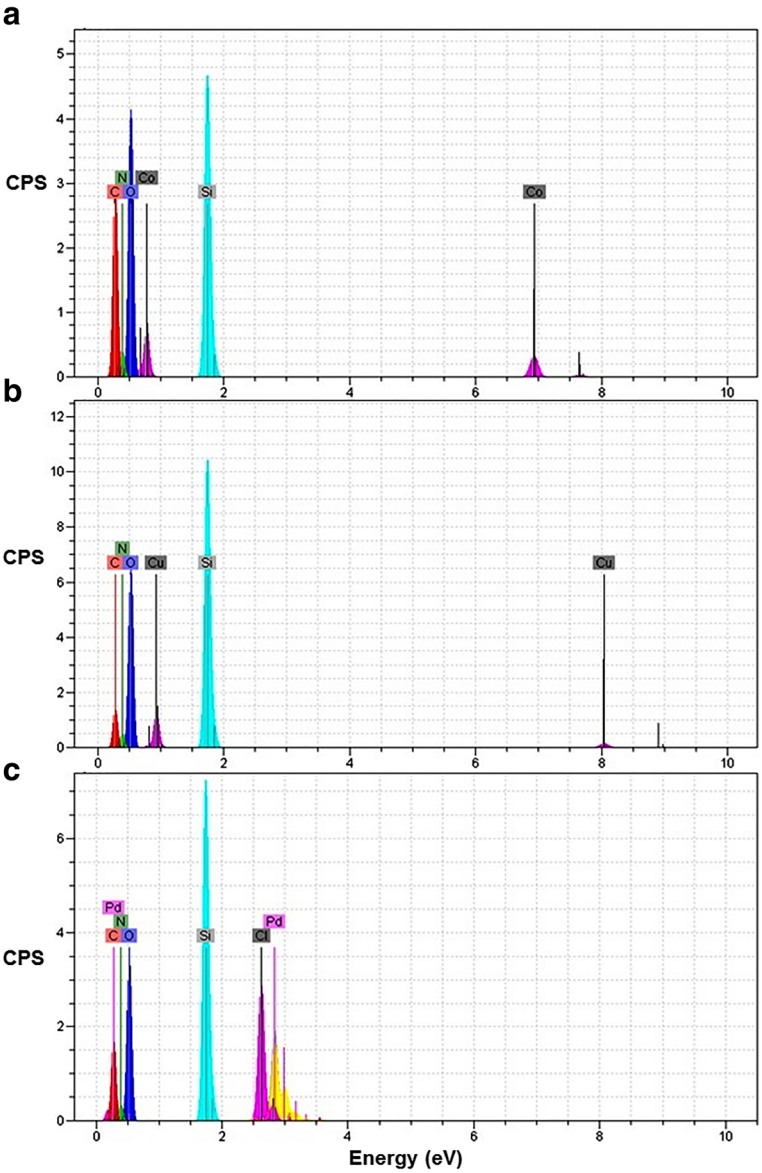

Fig. 4 EDX spectra of **a** MCM-41@PEI-Co, **b** MCM-41@PEI-Cu, and **c** MCM-41@PEI-Pd

13.2:9.1:15.6:12.9 for chelated Co, Cu, and Pd, respectively. Hence, divalent metal ions were successfully coordinated to the MCM-41@PEI supports.

Characterization of Immobilized Lipase on MCM-41@PEI-M

Several groups have considered the immobilization of lipase by metal chelated supports through the bonding of metal ions to the peripheral amino acids of the enzyme [56–59]. Transition metal ions are considered strong Lewis acids that can interact with strong Lewis bases. Therefore, carboxyl groups located on the periphery of the enzyme could be chelated with divalent metal ions. Moreover, an additional binding can be predicted between the metal ions and alkaline amine groups present on the lipase surface [18]. The presence of a relatively high number of residues with polar side chains facilitates multipoint bonding between metal and amino acids based on ionic and coordinate interactions.

In this study, lipase immobilization could be accomplished by ionic interactions between the negatively charged side chains of amino acids of the enzyme and the protonated amino groups present in MCM-41@PEI. The subsequent formation of coordinates between divalent metals and electron-donor groups present on the lipase surface could further improve the affinity of the enzyme for immobilization on MCM-41@PEI-M.

The time needed for optimum lipase immobilization onto MCM-41@PEI-M was estimated indirectly by measuring the relative activity of lipase versus time (Fig. 5a**)**. MCM-41@PEI-Co and MCM-41@PEI-Cu both reached optimum immobilization loading 60 min after the commencement of stirring with TLL in 100 mM citrate-phosphate buffer (pH 7), whereas for MCM-41@PEI-Pd immobilization took 90 min. The maximum IY of 75 ± 3.5% and IE of 65 ± 2.7% were obtained for MCM-41@PEI-Co, followed by MCM-41@PEI-Cu (IY = 70 ± 2.9% and IE = 60 ± 2.8%) and MCM-41@PEI-Pd (IY = 63 ± 2.8% and IE = 55 ± 3.6%).

pH and Temperature of Free and Immobilized Lipase

The activity of the free and immobilized lipase was examined at various pH values (pH 3–10) at 37 °C using citrate-phosphate, Tris-HCl, and glycine-NaOH buffers. The activity profiles of free and immobilized lipase are shown in Fig. 5b. Based on the results, lipase immobilized onto metal chelated supports showed better activity across a wide pH range. Metal ions play a critical role in maintaining enzyme stability at different pH values by cross-linking between PEI and lipase. Moreover, the buffering capacity of PEI due to the presence of a high number of secondary amine groups can enhance the lipase activity against pH variability [60]. The immobilized lipase showed higher activity at acidic pH values than free lipase. At lower pH, the available PEI amine groups would be protonated and able to attract hydroxide ions existing in the reaction medium. Thus, the microenvironmental pH around the lipase will be maintained at a higher pH than in the bulk medium, thus reducing the harsh, denaturing effects of acidic pH. This could explain why the immobilized lipase showed improved activity compared to the free enzyme at low pH. The optimum pH value for all metal chelated supports was around neutral pH, implying a probable interaction between His and metal ions, in which both protons of the imidazolium ion could be replaced by strong Lewis acids (i.e., divalent cations).

The optimum temperature for lipase activity was obtained by conducting the catalytic reaction at various temperatures between 15 and 75 °C (Fig. 5c). The immobilized lipase showed better activity over a wide range of temperatures compared to free lipase, except for

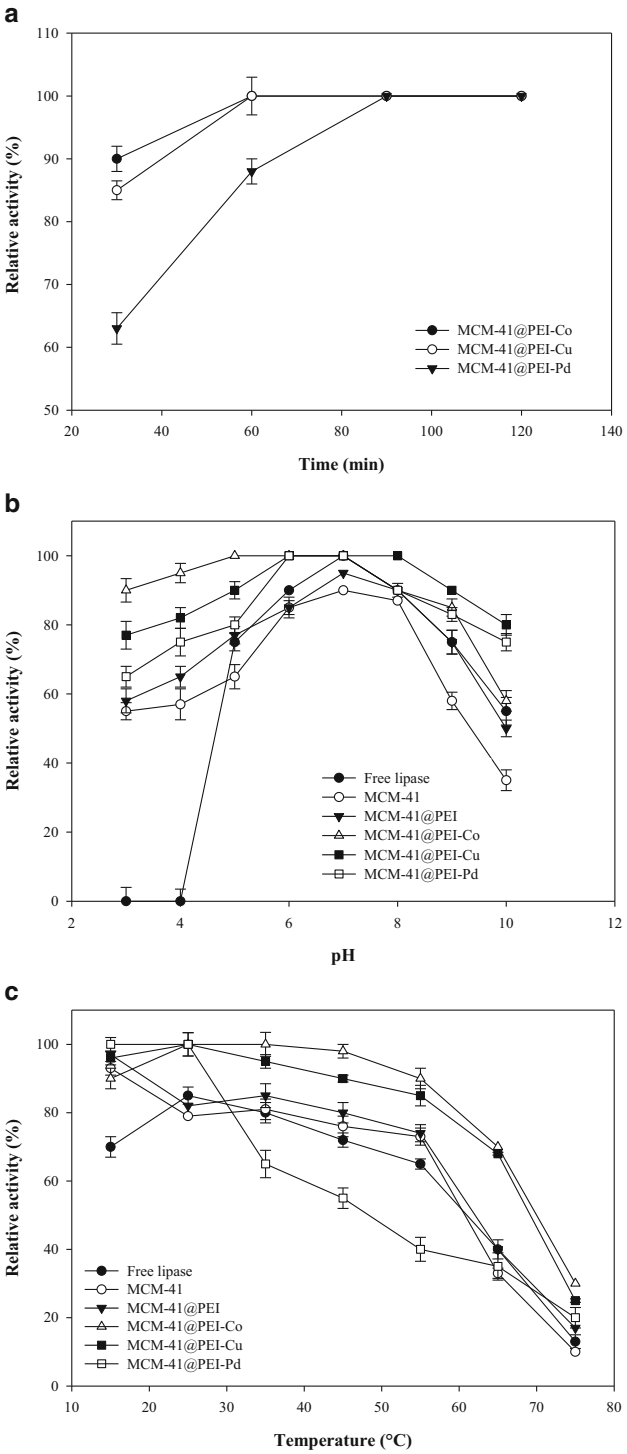

Fig. 5 **a** Time, **b** pH, and **c** temperature stability of free and immobilized lipase on the supports

MCM-41@PEI-Pd, where activity quickly decreased when the temperature exceeded 25 °C. Based on the temperature profile, immobilized lipase exhibited more than 90% of optimum activity at 15 °C irrespective of the metal chelate type, while free lipase only performed at 70% of its optimum activity. Higher catalytic activity for the immobilized lipase at lower temperatures could be considered as advantageous in industrial applications. Mass transfer is restricted at low temperatures, which avoid the substrate accessibility to the free lipase, while substrate interaction with active site of immobilized enzyme is more favorable. Da Silva et al. [61] and Wang et al. [62] have reported the same phenomenon. The only slightly higher activity for the immobilized lipase at elevated temperatures may be caused by the support constraining the conformational structure.

Reusability and Storage Stability of Free and Immobilized Lipase

Enzyme recycling after multiple catalytic operations was examined for immobilized lipase on MCM-41, MCM-41@PEI, and MCM-41@PEI-M. Figure 6a shows the number of successful catalytic cycles by the immobilized lipases against their retained activity. MCM-41@PEI and MCM-41 maintained 80 and 65% of their initial activities after 12 runs, while MCM-41@PEI-M lost approximately 80% of their activity at the final run. MCM-41@PEI performed as the best support in terms of the highest stability after multiple catalysis and washing steps. PEI is considered a hyperbranched polycationic network that establishes efficient electrostatic interactions between protonated amines and lipase [63]. Furthermore, the formation of a molecular cage arising from hydrogen bonds between PEI and lipase surface amino acids like Cys resulted in enzyme resistance after multicycle catalysis [60]. The high reusability capacity observed for the immobilized enzyme could be attributed to the protection of the biocatalyst in nanometric pores of the support [64]. The hydrodynamic radius of TLL based on tryptophan fluorescence spectroscopy [65] and crystallographic structures [66] has been estimated as 2.8 nm. This means lipase cannot become entrapped completely in the pores of MCM-41, and enzyme entrapment in the polymer network as well as enzyme adsorption by metal chelation play a crucial role to enhance the stability of the enzyme.

Based on hard-soft acid based rule (HSAB), Co^{+2} and Cu^{+2} are categorized as borderline acids, while Pd^{+2} considered as soft acid. The amine group existed in PEI and enzyme accounts for hard alkali, which provides less stable ligation between amine with Pd^{+2} compared to Co^{+2} and Cu^{+2} chelates [67, 68]. This means that after each washing step, the chance of losing metal linkage followed the order of MCM-41@PEI-Pd > MCM-41@PEI-Cu > MCM-41@PEI-Co (Fig. 6a). Consequently, it seems that entrapped enzyme in polymeric shell exhibited more stable catalytic activity compared to the enzyme immobilized by metal chelation due to the more enzyme protection against washing steps.

Free and immobilized lipases were stored at 25 °C, and their activities were monitored over 14 days. Figure 6b illustrates that immobilization increased the storage stability of TLL unlike free lipase. Generally, the structural stability of a free enzyme in solution will gradually decrease with prolonged storage time, while long-term stability can be achieved by enzyme confinement. According to Fig. 6b, the free lipase lost 90% of its activity over the 14 days. In contrast, the immobilized lipase onto MCM-41@PEI and MCM-41@PEI-Co displayed the highest storage stability among all other supports. Effective interactions between the amino groups of PEI and amino acids of lipase, as well as formation of stable cobalt-amino acid chelates could be responsible for the higher reusability. In addition, MCM-41, MCM-41@PEI-Cu, and MCM-41@PEI-Pd retained more than 50–55% of their initial activity during the same period. It could be concluded that lipase immobilization by cobalt-chelated support improves the storage stability of lipase at room temperature.

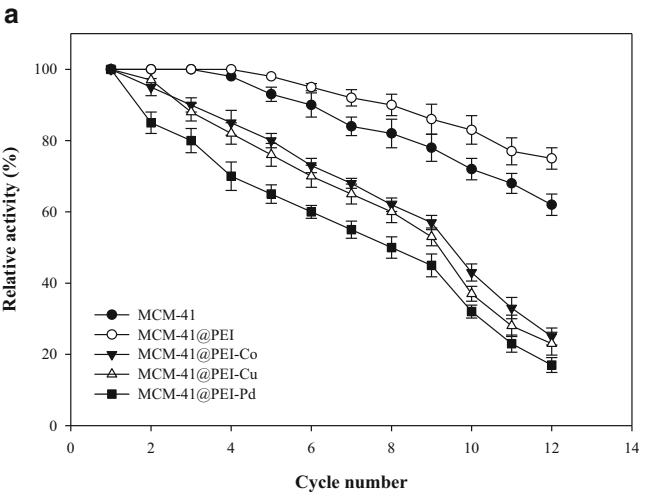
a
Relative activity (%)
Cycle number
MCM-41
MCM-41@PEI
MCM-41@PEI-Co
MCM-41@PEI-Cu
MCM-41@PEI-Pd

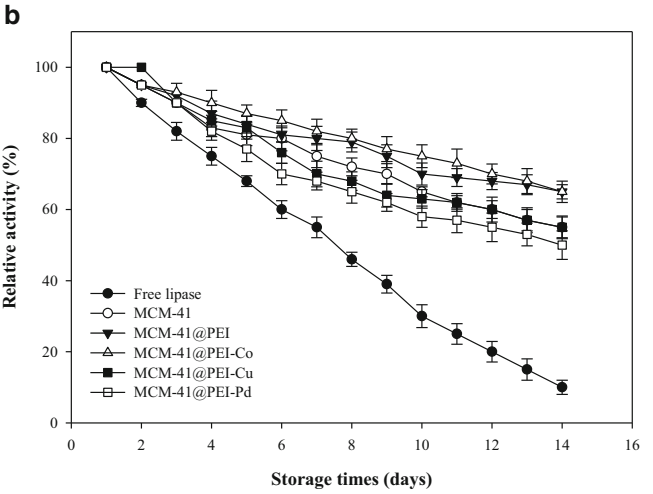
b
Relative activity (%)
Storage times (days)
Free lipase
MCM-41
MCM-41@PEI
MCM-41@PEI-Co
MCM-41@PEI-Cu
MCM-41@PEI-Pd

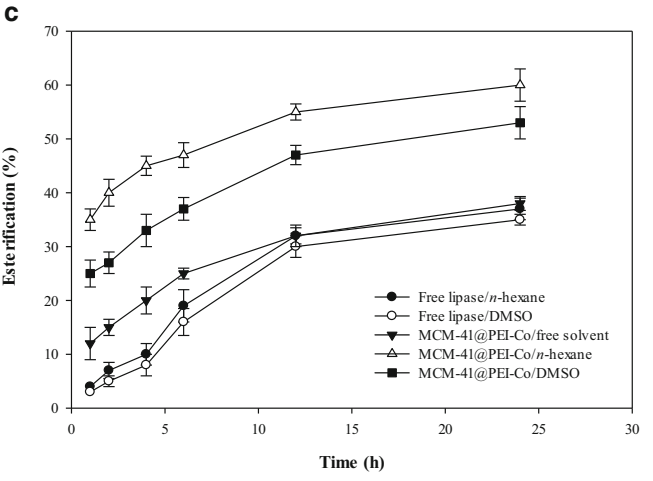
c
Esterification (%)
Time (h)
Free lipase/n-hexane
Free lipase/DMSO
MCM-41@PEI-Co/free solvent
MCM-41@PEI-Co/n-hexane
MCM-41@PEI-Co/DMSO

◀ **Fig. 6** **a** Reusability and **b** storage profiles of lipase immobilized on the supports. **c** Conversion of valeric acid in the presence of ethanol using free and immobilized lipase on MCM-41@PEI-Co in aqueous and nonaqueous media

Esterification Studies

The ability of free and immobilized lipase for the preparation of flavor esters from ethanol and valeric acid was investigated. The suggested mechanism for lipase-mediated esterification is formation of a tetrahedral acyl-lipase intermediate initiated by valeric acid reaction with the enzyme. Subsequently, a water molecule is released and ethanol binds to acyl-enzyme. The latter is transformed into a lipase–ester complex, followed by the ester leaving and recovery of free lipase for the next catalytic turn [69].

The yield of ethyl valerate formation using non-immobilized lipase in aqueous media was 23% when the valeric acid to alcohol molar ratio was 4:1 at 45 °C (data not shown). Esterification reactions were performed by immobilized lipase on MCM-41@PEI-Co to determine the advantage of immobilized lipase over free lipase. Figure 6c shows the results of esterification reactions carried out in DMS, *n*-hexane, and aqueous media for up to 24 h. Based on the results, there was an approximately 35% yield for esterification assisted by immobilized enzyme in aqueous media, which means immobilized lipase had no superior catalytic activity than its free counterpart in aqueous media. However, lipase immobilized onto MCM-41@PEI-Co had a significantly higher yield of 60% in *n*-hexane compared to free lipase (approximately 35%). An improved yield was also obtained in DMSO. The higher yield of esterification obtained in organic media could be due to the esters transferring into the organic phase, which may lead to a shift in equilibrium promoting ester production. Furthermore, non-immobilized lipase showed lower activity than immobilized enzyme due to the agglomeration of the free enzyme in organic media, which limits active site accessibility. Adlercreutz [13] proposed that the free form of lipase is nearly insoluble in organic solvents, and this prevents mass transfer during reaction, while immobilization improves the catalytic potential by stabilizing the enzyme structure. The same concept regarding the improved catalytic activity of immobilized lipase compared to the free enzyme in organic media has been previously reported [56, 69–72].

Conclusion

In this work, lipase was successfully immobilized through electrostatic, dipole-dipole, and hydrogen bonding interactions onto PEI-grafted MCM-41. Additionally, lipase was immobilized through chelated divalent metal ions that acted as a gentle cross-linker between PEI and the enzyme. The affinity of three divalent metal ions (Co^{2+}, Cu^{2+}, and Pd^{2+}) for TLL adsorption on MCM-41@PEI-M and the performance of the catalyst for apple flavor preparation were studied. Metal ions increased the capacity for enzyme immobilization, while the cobalt-assisted support displayed greater stability and reusability than the other metals. Compared to free lipase, the storage stability of immobilized lipase was improved, retaining its relative enzymatic activity over wide ranges of temperature and pH. Immobilized lipase onto MCM-41@PEI-Co exhibited an esterification yield of up to 60% against the free enzyme counterpart due to the limited activity of non-immobilized lipase in organic solvents. A higher esterification yield for an immobilized enzyme is highly favorable for industrial applications, which extensively use nonpolar substrates in organic chemical synthesis. With these desired features, this simple and efficient combinative immobilization strategy could be applied to

immobilize other industrially important enzymes as well as protein separation by affinity chromatography. Moreover, the prepared support could be introduced as a useful carrier for drug delivery, as sorbent for contaminant removal, and catalyst.

Acknowledgements This work was supported financially by the grants from Tehran University of Medical Sciences, and Iran National Science Foundation (INSF) Tehran, Iran.

References

1. Khoobi, M., Khalilvand-Sedagheh, M., Ramazani, A., Asadgol, Z., Forootanfar, H., & Faramarzi, M. A. (2014). Synthesis of polyethyleneimine (PEI) and β-cyclodextrin grafted PEI nanocomposites with magnetic cores for lipase immobilization and esterification. *Journal of Chemical Technology and Biotechnology, 91*, 375–384.
2. Khoobi, M., Motevalizadeh, S. F., Asadgol, Z., Forootanfar, H., Shafiee, A., & Faramarzi, M. A. (2014). Synthesis of functionalized polyethylenimine-grafted mesoporous silica spheres and the effect of side arms on lipase immobilization and application. *Biochemical Engineering Journal, 88*, 131–141.
3. Khoobi, M., Motevalizadeh, S. F., Asadgol, Z., Forootanfar, H., Shafiee, A., & Faramarzi, M. A. (2015). Polyethyleneimine-modified superparamagnetic Fe_3O_4 nanoparticles for lipase immobilization: characterization and application. *Materials Chemistry and Physics., 149*, 77–86.
4. Motevalizadeh, S. F., Khoobi, M., Shabanian, M., Asadgol, Z., Faramarzi, M. A., & Shafiee, A. (2013). Polyacrolein/mesoporous silica nanocomposite: synthesis, thermal stability and covalent lipase immobilization. *Materials Chemistry and Physics., 143*, 76–84.
5. Motevalizadeh, S. F., Khoobi, M., Sadighi, A., Khalilvand-Sedagheh, M., Pazhouhandeh, M., Ramazani, A., Faramarzi, M. A., & Shafiee, A. (2015). Lipase immobilization onto polyethylenimine coated magnetic nanoparticles assisted by divalent metal chelated ions. *Journal of Molecular Catalysis B: Enzymatic, 120*, 75–83.
6. Cesarini, S., Infanzón, B., Pastor, F. I. J., & Diaz, P. (2014). Fast and economic immobilization methods described for non-commercial *Pseudomonas* lipases. *BMC Biotechnology, 14*, 27–27.
7. DiCosimo, R., McAuliffe, J., Poulose, A. J., & Bohlmann, G. (2013). Industrial use of immobilized enzymes. *Chemical Society Reviews, 42*, 6437–6474.
8. Singh, R. K., Tiwari, M. K., Singh, R., & Lee, J. K. (2013). From protein engineering to immobilization: promising strategies for the upgrade of industrial enzymes. *International Journal of Molecular Sciences, 14*, 1232–1277.
9. Sadighi, A., & Faramarzi, M. A. (2013). Congo red decolorization by immobilized laccase through chitosan nanoparticles on the glass beads. *Journal of the Taiwan Institute of Chemical Engineers, 44*, 156–162.
10. Sun, X., Cai, X., Wang, R. Q., & Xiao, J. (2015). Immobilized trypsin on hydrophobic cellulose decorated nanoparticles shows good stability and reusability for protein digestion. *Analytical Biochemistry, 477*, 21–27.
11. Sheldon, R. A. (2007). Enzyme immobilization: the quest for optimum performance. *Advanced Synthesis & Catalysis, 349*, 1289–1307.
12. Zhang, Y., & Ji, C. (2010). Electro-induced covalent cross-linking of chitosan and formation of chitosan hydrogel films: its application as an enzyme immobilization matrix for use in a phenol sensor. *Analytical Chemistry, 82*, 5275–5281.
13. Adlercreutz, P. (2013). Immobilisation and application of lipases in organic media. *Chemical Society Reviews, 42*, 6406–6436.
14. Tang, Z., Luan, Y., Li, D., Du, H., Haddleton, D. M., & Chen, H. (2015). Surface immobilization of a protease through an inhibitor-derived affinity ligand: a bioactive surface with defensive properties against an inhibitor. *Chemical Communications, 51*, 10099–10102.
15. Porath, J., Carlsson, J., Olsson, I., & Belfrage, G. (1975). Metal chelate affinity chromatography, a new approach to protein fractionation. *Nature, 258*, 598–599.
16. Coulet, P., Carlsson, J., & Porath, J. (1981). Immobilization of enzymes on metal-chelate regenerable carriers. *Biotechnology and Bioengineering, 23*, 663–668.
17. Uzun, K., Çevik, E., Şenel, M., & Baykal, A. (2013). Reversible immobilization of invertase on Cu-chelated polyvinylimidazole-grafted iron oxide nanoparticles. *Bioprocess and Biosystems Engineering, 36*, 1807–1816.
18. Chen, T., Yang, W., Guo, Y., Yuan, R., Xu, L., & Yan, Y. (2014). Enhancing catalytic performance of β-glucosidase via immobilization on metal ions chelated magnetic nanoparticles. *Enzyme and Microbial Technology, 63*, 50–57.

19. Barbosa, O., Ortiz, C., Berenguer-Murcia, Á., Torres, R., Rodrigues, R. C., & Fernandez-Lafuente, R. (2015). Strategies for the one-step immobilization–purification of enzymes as industrial biocatalysts. *Biotechnology Advances, 33*(5), 435–456.
20. Uygun, D. A., Uygun, M., Akgöl, S., & Denizli, A. (2015). Reversible adsorption of catalase onto Fe^{3+} chelated poly (AAm-GMA)-IDA cryogels. *Materials Science and Engineering C, 50*, 379–385.
21. Woo, E. J., Kwon, H. S., & Lee, C. H. (2015). Preparation of nano-magnetite impregnated mesocellular foam composite with a Cu ligand for His-tagged enzyme immobilization. *Chemical Engineering Journal, 274*, 1–8.
22. Ghasemi, S., Sadighi, A., Heidary, M., Bozorgi-Koushalshahi, M., Habibi, Z., & Faramarzi, M. A. (2013). Immobilisation of lipase on the surface of magnetic nanoparticles and non-porous glass beads for regioselective acetylation of prednisolone. *IET Nanobiotechnology, 7*, 100–108.
23. Huang, S., Li, X., Xu, L., Ke, C., Zhang, R., & Yan, Y. (2015). Protein-coated microcrystals from *Candida rugosa* lipase: its immobilization, characterization, and application in resolution of racemic ibuprofen. *Applied Biochemistry and Biotechnology, 177*, 36–47.
24. Rauwerdink, A., & Kazlauskas, R. J. (2015). How the same core catalytic machinery catalyzes 17 different reactions: the serine-histidine-aspartate catalytic triad of α/β-hydrolase fold enzymes. *ACS Catalysis, 5*, 6153–6176.
25. Guo, S., Xu, J., Pavlidis, I. V., Lan, D., Bornscheuer, U. T., Liu, J., & Wang, Y. (2015). Structure of product-bound SMG1 lipase: active site gating implications. *FEBS Journal, 282*, 4538–4547.
26. Wang, Z., Li, S., Sun, L., Fan, J., & Liu, Z. (2013). Comparative analyses of lipoprotein lipase, hepatic lipase, and endothelial lipase, and their binding properties with known inhibitors. *PloS One, 8*, e72146.
27. Schrag, J. D., Li, Y., Wu, S., & Cygler, M. (1991). Ser-His-Glu triad forms the catalytic site of the lipase from *Geotrichum candidum*. *Nature, 351*, 761–764.
28. Brady, L., Brzozowski, A. M., Derewenda, Z. S., Dodson, E., Dodson, G., Tolley, S., Turkenburg, J. P., Christiansen, L., Huge-Jensen, B., Norskov, L., Thim, L., & Menge, U. (1990). A serine protease triad forms the catalytic Centre of a triacylglycerol lipase. *Nature, 343*, 767–770.
29. Aouf, C., Durand, E., Lecomte, J., Figueroa-Espinoza, M. C., Dubreucq, E., Fulcrand, H., & Villeneuve, P. (2014). The use of lipases as biocatalysts for the epoxidation of fatty acids and phenolic compounds. *Green Chemistry, 16*, 1740–1754.
30. Drozdz, A., Erfurt, K., Bielas, R., & Chrobok, A. (2015). Chemo-enzymatic Baeyer-Villiger oxidation in the presence of *Candida antarctica* lipase B and ionic liquids. *New Journal of Chemistry, 39*, 1315–1321.
31. Yuryev, R., Strompen, S., & Liese, A. (2011). Coupled chemo(enzymatic) reactions in continuous flow. *Beilstein Journal of Organic Chemistry, 7*, 1449–1467.
32. Rønne, T. H., Yang, T., Mu, H., Jacobsen, C., & Xu, X. (2005). Enzymatic interesterification of butterfat with rapeseed oil in a continuous packed bed reactor. *Journal of Agricultural and Food Chemistry, 53*, 5617–5624.
33. Shuai, W., Das, R. K., Naghdi, M., Brar, S. K., Verma, M. (2016). *A review on the important aspects of lipase immobilization on nanomaterials*. In press. doi:10.1002/bab.1515.
34. Xie, W., & Ma, N. (2009). Immobilized lipase on Fe_3O_4 nanoparticles as biocatalyst for biodiesel production. *Energy & Fuels, 23*, 1347–1353.
35. Xie, W., & Wang, J. (2014). Enzymatic production of biodiesel from soybean oil by using immobilized lipase on Fe_3O_4 /poly (styrene-methacrylic acid) magnetic microsphere as a biocatalyst. *Energy & Fuels, 28*, 2624–2631.
36. Xie, W., & Wang, J. (2012). Immobilized lipase on magnetic chitosan microspheres for transesterification of soybean oil. *Biomass & Bioenergy, 36*, 373–380.
37. Xie, W., & Zang, X. (2016). Immobilized lipase on core–shell structured Fe_3O_4–MCM-41 nanocomposites as a magnetically recyclable biocatalyst for interesterification of soybean oil and lard. *Food Chemistry, 194*, 1283–1292.
38. Caro-Jara, N., Mundaca-Uribe, R., Zaror-Zaror, C., Carpinelli-Pavisic, J., Aranda-Bustos, M., & Peña-Farfal, C. (2013). Development of a bienzymatic amperometric glucose biosensor using mesoporous silica (MCM-41) for enzyme immobilization and its application on liquid pharmaceutical formulations. *Electroanalysis, 25*, 308–315.
39. Gibson, L. (2014). Mesosilica materials and organic pollutant adsorption: part A removal from air. *Chemical Society Reviews, 43*, 5163–5172.
40. Hoffmann, F., Cornelius, M., Morell, J., & Fröba, M. (2006). Silica-based mesoporous organic–inorganic hybrid materials. *Angewandte Chemie International Edition, 45*, 3216–3251.
41. Egodawatte, S., Datt, A., Burns, E. A., & Larsen, S. C. (2015). Chemical insight into the adsorption of chromium(iii) on iron oxide/mesoporous silica nanocomposites. *Langmuir, 31*, 7553–7562.
42. Gao, Y., Xu, D., & Kispert, L. D. (2015). Hydrogen bond formation between the carotenoid canthaxanthin and the silanol group on MCM-41 surface. *Journal of Physical Chemistry B, 119*, 10488–10495.

43. He, C., Ren, L., Zhu, W., Xu, Y., & Qian, X. (2015). Removal of mercury from aqueous solution using mesoporous silica nanoparticles modified with polyamide receptor. *Journal of Colloid and Interface Science, 458*, 229–234.
44. Jiang, Y., Sun, W., Zhou, L., Ma, L., He, Y., & Gao, J. (2016). Improved performance of lipase immobilized on tannic acid-templated mesoporous silica nanoparticles. *Applied Biochemistry and Biotechnology, 179*, 1155–1169.
45. Tarn, D., Ashley, C. E., Xue, M., Carnes, E. C., Zink, J. I., & Brinker, C. J. (2013). Mesoporous silica nanoparticle nanocarriers: biofunctionality and biocompatibility. *Accounts of . Chemical Research, 46*, 792–801.
46. Wang, Y., Zhao, Q., Han, N., Bai, L., Li, J., Liu, J., Che, E., Hu, L., Zhang, Q., Jiang, T., & Wang, S. (2015). Mesoporous silica nanoparticles in drug delivery and biomedical applications. *Nanomedicine: Nanotechnology, Biology and Medicine, 11*, 313–327.
47. Tao, Y., Ju, E., Ren, J., & Qu, X. (2015). Bifunctionalized mesoporous silica-supported gold nanoparticles: intrinsic oxidase and peroxidase catalytic activities for antibacterial applications. *Advanced Materials, 27*, 1097–1104.
48. Bradford, M. M. (1976). A rapid and sensitive method for the quantitation of microgram quantities of protein utilizing the principle of protein-dye binding. *Analytical Biochemistry, 72*, 248–254.
49. Brzozowski, A. M., Savage, H., Verma, C. S., Turkenburg, J. P., Lawson, D. M., Svendsen, A., & Patkar, S. (2000). Structural origins of the interfacial activation in *Thermomyces (Humicola) lanuginosa* lipase. *Biochemistry, 39*, 15071–15082.
50. Saikia, B. J., & Parthasarathy, G. (2010). Fourier transform infrared spectroscopic characterization of kaolinite from Assam and Meghalaya. *Journal of Modern Physics, 1*, 206–210.
51. White, L. D., & Tripp, C. P. (2000). Reaction of (3-Aminopropyl)dimethylethoxysilane with amine catalysts on silica surfaces. *Journal of Colloid and Interface Science, 232*, 400–407.
52. Sutton, D., Durand, R., Shuai, X., & Gao, J. (2006). Poly (D, L-lactide-co-glycolide)/poly (ethylenimine) blend matrix system for pH sensitive drug delivery. *Journal of Applied Polymer Science, 100*, 89–96.
53. Helios, K., Wysokinski, R., Pietraszko, A., & Michalska, D. (2011). Vibrational spectra and reinvestigation of the crystal structure of a polymeric copper(II)–orotate complex, $[Cu(\mu\text{-}HOr)(H_2O)_2]n$: the performance of new DFT methods, M06 and M05-2X, in theoretical studies. *Vibrational Spectroscopy, 55*, 207–215.
54. Han, D., Li, C., & Chen, H. (1998). The assignment of Co-C bond stretching vibrational frequency of $CHsCo(DH)_2H_2O$ in IR and Raman spectra. *Spectroscopy lett, 31*, 1263–1277.
55. Drelinkiewicz, A., Hasik, M., Quillard, S., & Paluszkiewicz, C. (1999). Infrared and Raman studies of palladium—nitrogen-containing polymers interactions. *Journal of Molecular Structure, 511–512*, 205–215.
56. Kumar, A., Dhar, K., Kanwar, S. S., & Arora, P. K. (2016). Lipase catalysis in organic solvents: advantages and applications. *Biological Procedures Online, 18*, 1–11.
57. Haas, K. L., & Franz, K. (2009). Application of metal coordination chemistry to explore and manipulate cell biology. *Chemical Reviews, 109*, 4921–4960.
58. Alarcón-Payer, C., Pivetta, T., Choquesillo-Lazarte, D., González-Pérez, J. M., Crisponi, G., Castiñeiras, A., & Niclós-Gutiérrez, J. (2005). Thiodiacetato-copper (II) chelates with or without N-heterocyclic donor ligands: molecular and/or crystal structures of [Cu (tda)] n,[Cu (tda)$(Him)_2(H_2O)$] and [Cu (tda)(5Mphen)]·$2H_2O$ (Him = imidazole, 5Mphen = 5-methyl-1, 10-phenanthroline). *Inorganica Chimica Acta, 358*, 1918–1926.
59. Gaberc-Porekar, V., & Menart, V. (2001). Perspectives of immobilized-metal affinity chromatography. *Journal of Biochemical and Biophysical Methods, 49*, 335–360.
60. Zhang, Y., Ren, H., Wang, Y., Chen, K., Fang, B., & Wang, S. (2016). Bioinspired immobilization of glycerol dehydrogenase by metal ion-chelated polyethyleneimines as artificial polypeptides. *Scientific Reports, 6*, 24163.
61. Da Silva, V. C. F., Contesini, F. J., & Carvalho, P. O. (2008). Characterization and catalytic activity of free and immobilized lipase from *Aspergillus niger*: a comparative study. *Journal of the Brazilian Chemical Society, 19*, 1468–1474.
62. Wang, S.-G., Zhang, W.-D., Li, Z., Ren, Z.-Q., & Liu, H.-X. (2010). Lipase immobilized on the hydrophobic polytetrafluoroethene membrane with nonwoven fabric and its application in intensifying synthesis of butyl oleate. *Applied Biochemistry and Biotechnology, 162*, 2015–2026.
63. Schulz, C., Ludwig, R., & Gorton, L. (2014). Polyethyleneimine as a promoter layer for the immobilization of cellobiose dehydrogenase from *Myriococcum thermophilum* on graphite electrodes. *Analytical Chemistry, 86*, 4256–4263.
64. Ma, H., He, J., Evans, D. G., & Duan, X. (2004). Immobilization of lipase in a mesoporous reactor based on MCM-41. *Journal of Molecular Catalysis B: Enzymatic, 30*, 209–217.
65. Zhu, K., Jutila, A., Tuominen, E. K. J., & Kinnunen, P. K. J. (2001). Effects of i-propanol on the structural dynamics of *Thermomyces lanuginosa* lipase revealed by tryptophan fluorescence. *Protein Science, 10*, 339–351.

66. Swaminathan, R., Nath, U., Udgaonkar, J. B., Periasamy, N., & Krishnamoorthy, G. (1996). Motional dynamics of a buried tryptophan reveals the presence of partially structured forms during denaturation of barstar. *Biochemistry, 35*, 9150–9157.
67. Ueda, E. K. M., Gout, P. W., & Morganti, L. (2003). Current and prospective applications of metal ion-protein binding. *Journal of Chromatography A, 988*, 1–23.
68. Wang, Q., Cui, J., Guohui, L., Zhang, J., Huang, F., & Wei, Q. (2014). Laccase immobilization by chelated metal ion coordination chemistry. *Polymers, 6*, 2357–2370.
69. Stergiou, P. Y., Foukis, A., Filippou, M., Koukouritaki, M., Parapouli, M., Theodorou, L. G., Hatziloukas, E., Afendra, A., Pandey, A., & Papamichael, E. M. (2013). Advances in lipase-catalyzed esterification reactions. *Biotechnology Advances, 31*, 1846–1859.
70. Corbett, P. T., Leclaire, J., Vial, L., West, K. R., Wietor, J. L., Sanders, J. K. M., & Otto, S. (2006). Dynamic combinatorial chemistry. *Chemical Reviews, 106*, 3652–3711.
71. Gandhi, N. N., Patil, N. S., Sawant, S. B., Joshi, J. B., Wangikar, P. P., & Mukesh, D. (2000). Lipase-catalyzed esterification. *Catalysis Reviews, 42*, 439–480.
72. Torres, S., & Castro, G. R. (2004). Non-aqueous biocatalysis in homogeneous solvent systems. *Food Technology and Biotechnology, 42*, 271–277.